Towards quantifying global aerosol direct radiative effects using lidar: detection sensitivity

Tyler J. Thorsen[1], Richard A. Ferrare[1], Chris A. Hostetler[1], Mark A. Vaughan[1], and Qiang Fu[2]

[1]NASA Langley Research Center, Mail Stop 420, Hampton, Virginia, USA
[2]Department of Atmospheric Sciences, University of Washington, Seattle, Washington, USA

Key Points:

- The CALIPSO lidar does not detect all radiatively-significant aerosols
- This causes an underestimation of the aerosol direct radiative effect globally
- The detection sensitivity needed to derive the aerosol direct radiative effect accurately is determined

Corresponding author: Tyler J. Thorsen, `tyler.thorsen@nasa.gov`

Abstract

Spaceborne lidar observations have great potential to provide accurate global estimates of the aerosol direct radiative effect (DRE) in both clear and cloudy conditions. However, comparisons between observations from the Cloud-Aerosol Lidar and Infrared Pathfinder Satellite (CALIPSO) and multiple years of Atmospheric Radiation Measurement (ARM) program's ground-based Raman lidars (RL) show that CALIPSO does not detect all radiatively-significant aerosol, i.e. aerosol that directly modifies the Earth's radiation budget. We estimated that using CALIPSO observations results in an underestimate of the magnitude of the global mean aerosol DRE by up to 54%. The ARM RL datasets along with NASA Langley airborne high spectral resolution lidar (HSRL) data from multiple field campaigns are used to compute the detection sensitivity required to accurately resolve the aerosol DRE. This shows that a lidar with a backscatter coefficient detection sensitivity of about $1-2x10^{-4}km^{-1}sr^{-1}$ at 532nm would resolve all the aerosol needed to derive the DRE to within 1%.

1 Introduction

Assessing and interpreting the Earth's changing radiative energy budget continues to be hampered by large uncertainties in clouds and aerosols [*Boucher et al.*, 2013]. For aerosols, the most basic understanding starts with knowledge of how they affect the Earth's radiation balance in the present climate. Many studies [*Yu et al.*, 2006, and references therein] have used the aerosol optical depth (AOD) retrieved from passive remote sensors to make estimates of the shortwave (SW) aerosol direct radiative effect (DRE), i.e. the radiative perturbation due to aerosols both natural and anthropogenic. These studies focus on the SW aerosol DRE since passive remote sensing cannot provide the vertical information nor nighttime observations needed to determine the longwave (LW) aerosol DRE [*Torres et al.*, 2007; *Chand et al.*, 2008; *Zarzycki and Bond*, 2010]. Accurate estimates of SW aerosol DRE from passive remote sensors are often limited to daytime cloud-free ocean since it is under these conditions that passive aerosol retrievals perform best [*Li et al.*, 2009; *Kokhanovsky et al.*, 2010]. While advances have been made in passive sensor retrieval over cloud [*Torres et al.*, 2007; *Waquet et al.*, 2009, 2013; *de Graaf et al.*, 2012; *Jethva et al.*, 2013; *Meyer et al.*, 2015] and land [*Dubovik et al.*, 2011; *Lyapustin et al.*, 2011a,b], complete global all-sky aerosol DRE estimates, even after the combination of multiple techniques, must rely on model information to fill in the inevitable gaps [e.g. *Lacagnina et al.*, 2017].

The advent of the lidar on board the Cloud-Aerosol Lidar and Infrared Pathfinder Satellite (CALIPSO) [*Winker et al.*, 2009, 2010] alleviates these aforementioned limitations of passive sensors. CALIPSO provides vertically-resolved aerosol properties over all surface types during both day and night, and can more accurately separate cloud from aerosol in the same profile [*Liu et al.*, 2009]. Recognizing these advantages, recent studies have used CALIPSO to provide new all-sky estimates of the global TOA SW aerosol DRE [*Oikawa et al.*, 2013; *Matus et al.*, 2015]. Notably, the clear-sky ocean aerosol DRE from these CALIPSO-based estimates [*Oikawa et al.*, 2013; *Matus et al.*, 2015] are significantly smaller in magnitude than the passive sensor-based ones [*Yu et al.*, 2006].

Validating CALIPSO relative to advanced ground-based or airborne lidars that directly measure the extinction profile allows for the separation of CALIPSO errors due to assumed lidar ratios (the ratio of extinction to backscatter) and those errors from undetected aerosol. Unfortunately, these advanced lidars have compiled very few extended datasets that can be used for long-term CALIPSO validation, and thus comparisons are often limited to case studies [e.g. *Pappalardo et al.*, 2010]. Only recently has more rigorous CALIPSO validation been possible by compiling data from multiple flights of the airborne NASA Langley high spectral resolution lidar (HSRL) [*Hair et al.*, 2008] and through a re-processing [*Thorsen et al.*, 2015; *Thorsen and Fu*, 2015a] of the continuous-operated DOE Atmospheric Radiation Measurement (ARM) program's Raman lidars (RL) [*Goldsmith et al.*, 1998; *Ferrare et al.*, 2006; *Newsom*, 2009]. Studies using these HSRL and Raman lidar datasets have doc-

umented that optically-thinner aerosol can go undetected by CALIPSO [*Kacenelenbogen et al.*, 2014; *Rogers et al.*, 2014; *Thorsen et al.*, 2015].

Thorsen and Fu [2015b] (hereafter TF15) assessed CALIPSO's ability to detect all radiatively-significant aerosol, i.e. aerosol that directly modifies the TOA radiation budget, using multiple years of data from the ARM RLs. TF15 showed that the aerosol that goes undetected by CALIPSO is radiatively-significant and results in an underestimate in the magnitude of the SW aerosol DRE by 30–50% at the two ARM sites examined. In this study, we first examine biases in the new version 4 of the CALIPSO data (section 3) following TF15. We then assess how well the biases found over the two ground sites can characterize the biases present in the global CALIPSO data set (section 4). The ARM RL data along with data from the airborne NASA Langley HSRL are used to compute the detection sensitivity required for a lidar to fully-resolve radiatively-significant aerosol (section 5) and we conclude by discussing how future space-based lidars might improve our knowledge of aerosol radiative effects (section 6).

2 Datasets

Three lidar datasets are used in this study:

1. the CALIPSO satellite [*Winker et al.*, 2009, 2010] level 2 version 3 (v3) and version 4 (v4) vertical feature mask (VFM) product and the aerosol layer (ALay) product,
2. multiple years of ARM RL data acquired at the Tropical Western Pacific (TWP) site in Darwin, Australia and the Southern Great Plains (SGP) site in Oklahoma, and subsequently analyzed using the RL Feature detection and EXtinction retrieval (RL-FEX) algorithm [*Thorsen et al.*, 2015; *Thorsen and Fu*, 2015a], and
3. the NASA Langley HSRL [*Hair et al.*, 2008] data from multiple campaigns across North America.

Direct comparisons are made between collocated RL-FEX and CALIPSO data. We focus on the subset of profiles that are "transparent", i.e. profiles where the laser beam penetrates completely through all cloud and aerosol layers, and "cloud-free" profiles, profiles that are both transparent and have no cloud layers detected. Full descriptions of datasets, collocation criteria, and the sub-setting of profiles can be found in the Supporting Information (Text S1).

3 CALIPSO biases over the ARM sites

Profiles of RL-FEX and CALIPSO aerosol occurrence (number of aerosol / (number of aerosol + number of clear)) in transparent and cloud-free profiles are shown in Fig. 1. Overall, significantly less aerosol is detected by CALIPSO relative to RL-FEX at both the SGP and TWP sites. As expected, CALIPSO's detection is better during the nighttime (dashed lines) than daytime (dotted lines) and improved when the comparison is limited to cloud-free profiles only (Fig. 1(c)-(d)). However, even in the best-case scenario of cloud-free nighttime profiles, CALIPSO detects less aerosol than RL-FEX. Aerosol occurrence slightly increases in CALIPSO v4 (red) over CALIPSO v3 (gray) with the exception of a few heights in the daytime TWP profiles. This is likely due to improved calibration in v4 that increases the magnitude of the backscatter [*Getzewich et al.*, 2016] allowing for the detection of more tenuous layers.

Using the newer CALIPSO v4 data, we perform a similar analysis to TF15 to assess how well CALIPSO detects all radiatively-significant aerosol. Unlike TF15, we do not perform radiative transfer calculations but instead we assess AOD biases. Since AODs are typically relatively small, the aerosol DRE depends linearly on the AOD so relative biases in the DRE and AOD are expected to be similar. Therefore, fully resolving the AOD is akin to detecting all radiatively-significant aerosol. The effect of detection sensitivity on the AOD

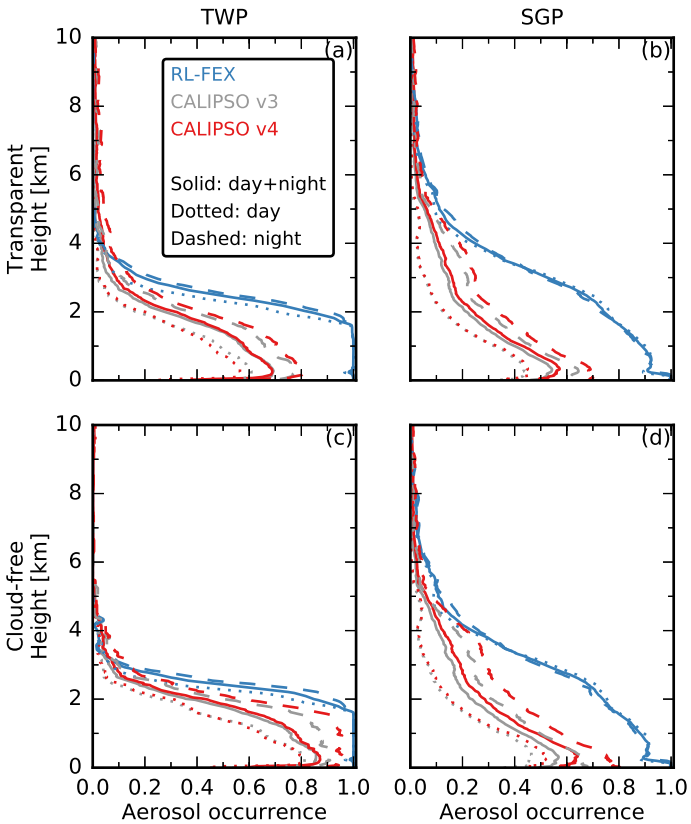

Figure 1. The aerosol occurrence (number of aerosol / (number of aerosol + number of clear)) in (a,b) transparent and (c,d) cloud-free profiles from RL-FEX (blue), version 3 (gray) and version 4 (red) of the CALIPSO VFM v4 product at the (a,c) TWP and (b,d) SGP sites. Profiles are also shown separately for the daytime (dotted) and nighttime (dashed) observations.

is isolated by generating a set of RL-FEX data that has been degraded to CALIPSO's sensitivity (Supporting Information, Text S2). This procedure also accounts for the difference in wavelength between the RL systems and CALIPSO (355 nm and 532 nm, respectively). Biases from aerosol undetected by CALIPSO are assessed by comparing the original RL-FEX data to the simulated CALIPSO-like data.

AOD biases due to aerosol undetected by CALIPSO are shown in Fig. 2. Overall AOD is substantially underestimated by CALIPSO, thus demonstrating that CALIPSO's detection sensitivity is not sufficient for detecting all radiatively-significant aerosol that occurs over the SGP and TWP sites. The AOD is underestimated by 27% (49%) at TWP (SGP) in transparent profiles. The use of v4 CALIPSO data reduces the magnitude of the biases in Fig. 2 by an average of 3% over using v3 CALIPSO data (not shown). Also shown is the portion of the AOD bias due to all aerosol going completely undetected in the profile, i.e. CALIPSO AOD = 0 (hatched bars in Fig. 2). Comparing this to the total biases shows that most of CALIPSO's bias is due to the partial detection of aerosols in a profile rather than all aerosol going completely undetected.

4 Global implications of CALIPSO biases

Although we can only directly evaluate CALIPSO's sensitivity using the RL-FEX data over the two ARM sites, understanding how these two comparisons represent global biases is

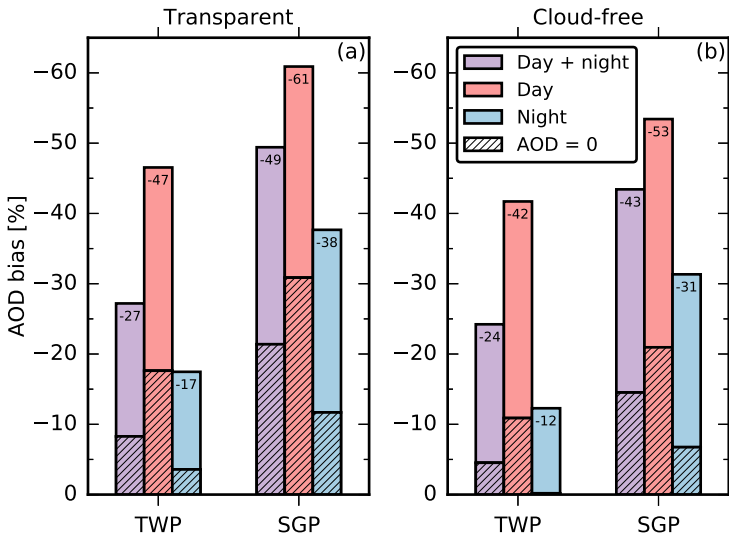

Figure 2. CALIPSO aerosol optical depth (AOD) biases due to undetected aerosol for (a) transparent and (b) cloud-free profiles over the ARM TWP and SGP sites shown separate for both day and night (purple), day only (red), and night only (blue). The hatched portion of each bar denotes the portion of the AOD bias caused by all aerosol going complete undetected by CALIPSO in a profile (i.e. CALIPSO AOD = 0).

highly desirable. Their global-scale representativeness depends on the similarity of the vertical profiles of aerosol extinction and backscatter, overlying transparent cloud optical depths, and the magnitude of the solar background. Determining the combined similarity from all these components is not straightforward. Instead, the frequency of zero AOD retrieved by CALIPSO, i.e. the frequency with which CALIPSO does not detect any aerosol in a profile, is used as an indicator of the total AOD bias. Doing this is supported by the high correlation ($r = 0.96$) of the total AOD bias (bars in Fig. 2) and the portion of the AOD bias caused by zero AOD shown (hatched segments of bars in Fig. 2). This correlation is to be expected if the undetected aerosol is predominately to due random noise: larger (smaller) amounts of noise should increase (decrease) both the total bias along with the bias that results from aerosol in a profile going completely undetected. The presumption of random noise is also supported by TF15 who showed that the distributions of undetected aerosol extinction coefficients are consistent with that expected from random noise.

It is expected that the true AOD should always be greater than zero since some amount of aerosols are always present. This is the case in the RL-FEX data where nearly all profiles (99.99%) have an AOD greater than zero. For the CALIPSO data over the two ARM sites the frequency of zero AOD is larger ranging from 0% in nighttime cloud-free profiles over TWP to 43% in daytime transparent profiles over SGP. Figure 3 shows the frequency of zero AOD in CALIPSO data is also significant over most of the globe. On average, 29% (17%) of transparent (cloud-free) CALIPSO profiles have zero AOD. Larger frequencies of zero CALIPSO AOD are found where detection is expected to be more difficult: during daytime, in the presence of clouds, over areas where aerosol is more vertically diffuse (land), and over brighter surfaces (land, and polar regions) where the solar background noise is larger. CALIPSO performs best in nighttime cloud-free profiles over ocean where the average frequency of zero AOD is 3%.

CALIPSO's frequency of zero AOD over the ARM sites (bracketed values in Fig. 3) typically encompasses the corresponding global mean values in Fig. 3. With the exception of the transparent nighttime comparison, the global mean frequency of zero AOD is close to the mean value of the two ARM sites. Therefore, the average of AOD biases at the two ARM

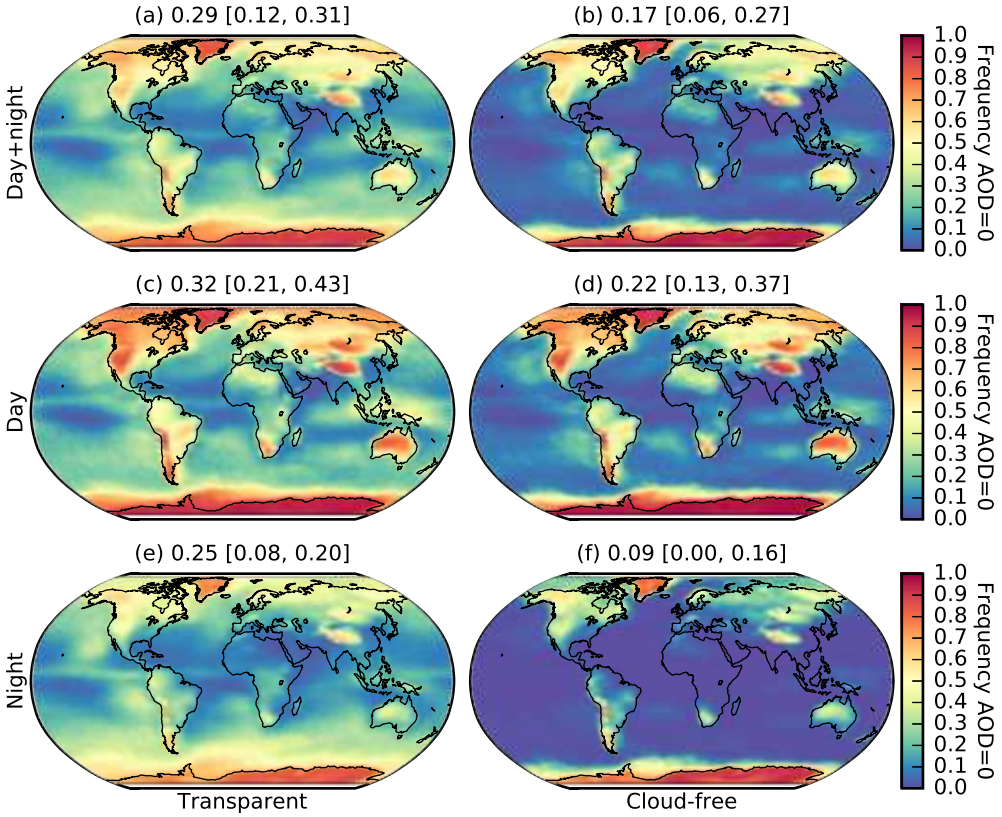

Figure 3. The frequency of no aerosol optical depth (i.e. AOD = 0) in the CALIPSO 5km ALay v4 product for (a,c,e) transparent and (b,d,f) cloud-free profiles during (a,b) both day and night, (c,d) day only, and (e,f) night only. The global mean frequency of AOD = 0 is given above each panel along with the range of the frequencies for the subset of profiles over the ARM TWP and SGP sites in brackets [TWP, SGP]. Average frequencies are shown on a 2° by 5° latitude by longitude grid from the period of June 2006 - November 2015.

sites in Fig. 2 can be used as a rough estimate of CALIPSO's global mean AOD bias. During the daytime, CALIPSO's global mean AOD bias is about -54% (-47%) in transparent (cloud-free) profiles. For nighttime cloud-free profiles, the bias is -22%. For transparent nighttime profiles the global mean frequency of zero AOD is more similar to that over the SGP site, but larger by 5%. Therefore, the AOD bias computed at the SGP site of -38% likely represents a lower bound on the CALIPSO global mean bias in nighttime transparent profiles.

5 Effect of lidar detection sensitivity on AOD bias

CALIPSO's limited sensitivity raises the question: what sensitivity does a lidar need to detect all radiatively-significant aerosols? To explore this, the RL-FEX data and the combination of data from 25 field campaigns performed by the NASA Langley airborne HSRL are used to compute the AOD bias that results from imposing various minimum detectable backscatter coefficient thresholds. The RL-FEX data is used to compute the true mean AOD at each ARM site. Relative to this true mean, the AOD bias from ignoring aerosols with backscatter coefficients below a certain threshold is computed. This is repeated for 60 different thresholds. The same processes is also performed with the NASA HSRL data. The usefulness of this exercise is made possible by our confidence in the ability of the ARM RL

and NASA HSRL to detect all aerosol that contribute significantly to the AOD (Supporting Information, Text S3).

The AOD bias as a function of the aerosol backscatter threshold is shown in Fig. 4. These AOD bias curves show a somewhat consistent dependence on the backscatter threshold among the three datasets. Figure 4 shows that if one, for example, wanted to resolve the AOD to within 5%, a lidar would need to be able to detect a minimum backscatter coefficient $5.6x10^{-4}km^{-1}sr^{-1}$ at 355 nm (or equivalently $3.5x10^{-4}km^{-1}sr^{-1}$ 532nm). Alternatively, a detection sensitivity of $1 - 2x10^{-4}km^{-1}sr^{-1}$ at 532nm would limit the AOD bias to within about -1% and hence be sufficient to resolve all aerosol needed to derive the DRE accurately.

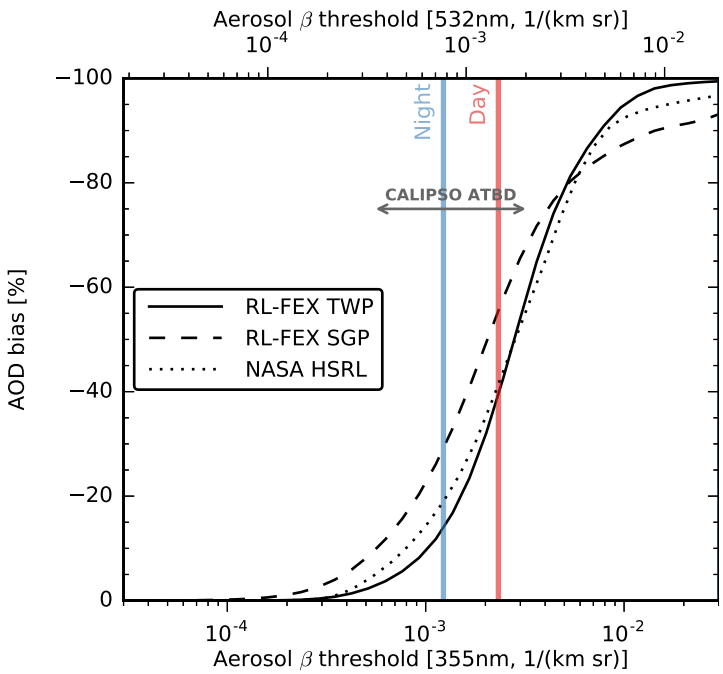

Figure 4. The aerosol optical depth (AOD) bias as a function of imposing a minimum detectable aerosol backscatter (β) threshold on the RL-FEX TWP (solid black), RL-FEX SGP (dashed black), and NASA Langley HSRL (dotted black) datasets. The NASA Langley HSRL is the compilation of 25 field campaigns (Fig. S1). The mean CALIPSO detection thresholds inferred from the comparison to the RL-FEX TWP and SGP data (section 3) are given as vertical lines for (red) day and (blue) night. The range of CALIPSO theoretical backscatter detection limits from the CALIPSO Algorithm and Theoretical Basis Document [ATBD, *Vaughan et al.*, 2005] are depicted as a double sided gray arrow. The bottom (top) x axis gives the backscatter at 355nm (532nm). These 355nm/532nm axes are offset using a backscatter color ratio of 1.60 (Supporting Information, Text S4)

Figure 4 also shows CALIPSO's average detection thresholds in cloud-free profiles inferred from the AOD bias analysis in section 4 (red and blue vertical lines). The theoretical detection limits of CALIPSO in cloud-free profiles from the CALIPSO Algorithm and Theoretical Basis Document [ATBD, *Vaughan et al.*, 2005] are depicted as a double sided gray arrow. This arrow spans the detection sensitivity for a nighttime scene with 80 km of horizontal averaging to a daytime scene with 5 km of averaging. Comparing this range to the thresholds derived in this work and in *Rogers et al.* [2014] along with the AOD biases reported by *Kim et al.* [2017] (Supporting Information, Text S5) shows that CALIPSO performance is generally consistent with its expected sensitivity.

6 Conclusions and the future of spaceborne lidar observations

Comparisons between CALIPSO and the ARM Raman lidar (RL) data over the TWP Darwin, Australia site and the SGP site in Oklahoma reveal that CALIPSO does not detect all radiatively-significant aerosol, i.e. aerosol that directly modifies the radiation budget. By extrapolating these comparisons, we show that this undetected aerosol causes CALIPSO to underestimate the global mean AOD (or equivalently the magnitude of the global mean aerosol direct radiative effect (DRE)) by approximately 54% (47%) in transparent (cloud-free) daytime profiles. During the nighttime, the AOD bias is about -22% in cloud-free profiles and is estimated to be at least -38% in transparent profiles. The ARM RL data along with data from multiple field campaigns of the airborne NASA Langley high spectral resolution lidar (HSRL) were used to compute the detection sensitivity required for a lidar to resolve all radiatively-significant aerosol. This analysis shows that a lidar with a backscatter coefficient detection sensitivity of about $1 - 2x10^{-4} km^{-1} sr^{-1}$ at 532nm would limit the AOD bias to within about -1% and hence be sufficient to resolve all aerosol needed to derive the DRE accurately.

Some improvements on the CALIPSO AOD biases presented here could be realized through the application of alternative retrieval methods [*Hu*, 2007; *Liu et al.*, 2015; *Josset et al.*, 2008; *Venkata and Reagan*, 2016]. The common feature of these methods is the use of the scattering properties of a known target, either opaque water clouds [*Hu*, 2007; *Liu et al.*, 2015] or the ocean surface [*Josset et al.*, 2008; *Venkata and Reagan*, 2016], to provide a column-constraint for the retrieval of AOD. While each method potentially provides more accurate AOD, they can only be applied in specific situations: over opaque water clouds [*Hu*, 2007; *Liu et al.*, 2015] or in clear-sky profiles over ocean [*Josset et al.*, 2008; *Venkata and Reagan*, 2016].

Recently, additional spaceborne lidar observations have been available from the Cloud-Aerosol Transport System [CATS, *McGill et al.*, 2015; *Yorks et al.*, 2016] lidar that operates on the International Space Station. However, the frequency of zero AOD in the CATS version 1.05 level 2 data is on average ~90% larger than CALIPSO (Fig. S3), an indication of an even poorer detection sensitivity than CALIPSO. EarthCARE, a soon to be launched joint ESA-JAXA satellite, will include a single-wavelength polarization-sensitive HSRL ATLID. ATLID is designed for improved daytime performance over CALIPSO, but its nighttime performance is expected to be comparable to CALIPSO [*Illingworth et al.*, 2015]. Since CALIPSO still underestimates the nighttime global mean AOD by 22% in cloud-free profiles and by at least 38% in transparent profiles, it is likely significant biases will remain in ATLID data. However, some improvement on ATLID's nominal detection limits may be possible from the advantages in processing a HSRL signal as described below.

While a spaceborne lidar has great potential to provide accurate global estimates of both shortwave and longwave aerosol DRE in all-sky conditions, the sensitivity of the current CALIPSO and CATS lidars and the expected sensitivity of ATLID on EarthCARE indicates that calculations of the aerosol DRE are, and will continue to be, significantly biased. The key requirement to eliminate these biases is a more sensitive lidar capable of fully-resolving all radiatively-significant aerosol. This requirement, among others, is being taken under consideration for the MESCAL (Monitoring the Evolving State of Clouds and Aerosol Layers) mission concept— a joint mission concept study between CNES and NASA Langley of a spaceborne HSRL. Rather than addressing this issue with a more sensitive version of an elastic backscatter lidar like CALIPSO, directly measured backscatter and extinction coefficients from an HSRL allows for larger amount of averaging (which reduces noise and improves sensitivity) to be safely performed. With an elastic backscatter lidar like CALIPSO, averaging attenuated backscatter is complicated by needing to correct for the non-linear attenuation without direct knowledge of the extinction profile. Therefore, larger amounts of averaging are increasingly error prone as signals with dissimilar amounts of attenuation are averaged. An HSRL also allows for accurate "full-column" retrievals that integrate the entire profile to obtain the column optical depth. This integration serves to greatly decrease noise

allowing for a very sensitive measurement of the AOD. AOD measured in this way would provide a built-in reference AOD for checking the accuracy of HSRL extinction profiles and could be added as an additional constraint in a detection algorithm.

Beyond extinction profiles, additional quantities are required for a radiative flux calculation: profiles of the aerosol single-scattering albedo (SSA), asymmetry parameter (g) and the wavelength dependence of the extinction coefficients. Currently, operational retrievals of these properties are not made globally, forcing calculations of aerosol DRE to make assumptions based on a limited knowledge of the aerosol type [e.g. *Oikawa et al.*, 2013; *Matus et al.*, 2015]. One of the mission concepts being developed for MESCAL is a instrument capable of measuring backscatter, extinction, and depolarization at multiple wavelengths. Measurements from such an instrument, when combined with additional column constraints provided by a multiwavelength multiangle polarimeter, has the potential to provide vertically-resolved retrievals of aerosol microphysical properties including SSA and g [*Müller et al.*, 2014; *Burton et al.*, 2016]. Observing these quantities globally would allow for a detailed look at aerosol DRE beyond the usual focus on the SW TOA effect: i.e. the radiative effects at the surface, within the atmosphere, and in the LW where estimates have been limited [*Bharmal et al.*, 2009; *Huang et al.*, 2009]. Current satellite observations also do not provide all the quantities needed to compute the aerosol direct radiative forcing (DRF), i.e. the radiative effect of just anthropogenic aerosols. A multiwavelength HSRL would also allow for a more refined aerosol classification to be made [*Burton et al.*, 2012; *Burton et al.*, 2014] enabling a better estimate of the anthropogenic aerosol radiative effect. These observations could better constrain the aerosol DRF whose uncertainty is large enough that its sign is unknown [*Boucher et al.*, 2013] which undermines our ability to model aerosol effects on climate.

Acknowledgments

The Raman lidar RL-FEX is available as an evaluation VAP from the ARM data archive (www.archive.arm.gov). The combined Raman and HSRL CHARMS dataset is available as a PI product from the ARM data archive. The CALIPSO datasets were obtained from the NASA Langley Research Center Atmospheric Science Data Center. We thank S.P. Burton for comments on this work and discussions on multiwavelength HSRL capabilities, and K.A. Powell whose MESCAL simulations help inspire this work. Thanks also to J.W. Hair for guidance on the NASA HSRL datasets. This research was supported by the NASA Aerosol-Clouds-Ecosystem (ACE) mission study program. Backscatter color ratio values were obtained using measurements acquired during the U.S. Dept. of Energy Atmospheric Research Program (ARM) Combined HSRL and Raman lidar Measurement Study (CHARMS) mission under Grant DE-SC0014042.

References

Bharmal, N. A., A. Slingo, G. J. Robinson, and J. J. Settle (2009), Simulation of surface and top of atmosphere thermal fluxes and radiances from the radiative atmospheric divergence using the ARM Mobile Facility, GERB data, and AMMA Stations experiment, *J. Geophys. Res.*, *114*, doi:10.1029/2008jd010504.

Boucher, O., D. Randall, P. Artaxo, C. Bretherton, G. Feingold, P. Forster, V.-M. Kerminen, Y. Kondo, H. Liao, U. Lohmann, P. Rasch, S. Satheesh, S. Sherwood, B. Stevens, and X. Zhang (2013), *Climate Change 2013: The Physical Science Basis. Contribution of Working Group I to the Fifth Assessment Report of the Intergovernmental Panel on Climate Change: Clouds and Aerosols*, chap. 7, pp. 571–658, Cambridge University Press, Cambridge, United Kingdom and New York, NY, USA, doi: 10.1017/CBO9781107415324.016.

Burton, S. P., R. A. Ferrare, C. A. Hostetler, J. W. Hair, R. R. Rogers, M. D. Obland, C. F. Butler, A. L. Cook, D. B. Harper, and K. D. Froyd (2012), Aerosol classification using airborne High Spectral Resolution Lidar measurements – methodology and examples, *Atmos. Meas. Tech.*, *5*(1), 73–98, doi:10.5194/amt-5-73-2012.

Burton, S. P., M. A. Vaughan, R. A. Ferrare, and C. A. Hostetler (2014), Separating mixtures of aerosol types in airborne High Spectral Resolution Lidar data, *Atmos. Meas. Tech.*, *7*(2), 419–436, doi:10.5194/amt-7-419-2014.

Burton, S. P., E. Chemyakin, X. Liu, K. Knobelspiesse, S. Stamnes, P. Sawamura, R. H. Moore, C. A. Hostetler, and R. A. Ferrare (2016), Information content and sensitivity of the $3\beta + 2\alpha$ lidar measurement system for aerosol microphysical retrievals, *Atmos. Meas. Tech.*, *9*(11), 5555–5574, doi:10.5194/amt-9-5555-2016.

Chand, D., T. L. Anderson, R. Wood, R. J. Charlson, Y. Hu, Z. Liu, and M. Vaughan (2008), Quantifying above-cloud aerosol using spaceborne lidar for improved understanding of cloudy-sky direct climate forcing, *J. Geophys. Res.*, *113*(D13), doi:10.1029/2007jd009433.

de Graaf, M., L. G. Tilstra, P. Wang, and P. Stammes (2012), Retrieval of the aerosol direct radiative effect over clouds from spaceborne spectrometry, *J. Geophys. Res.*, *117*(D7), doi:10.1029/2011jd017160.

Dubovik, O., M. Herman, A. Holdak, T. Lapyonok, D. Tanré, J. L. Deuzé, F. Ducos, A. Sinyuk, and A. Lopatin (2011), Statistically optimized inversion algorithm for enhanced retrieval of aerosol properties from spectral multi-angle polarimetric satellite observations, *Atmos. Meas. Tech.*, *4*(5), 975–1018, doi:10.5194/amt-4-975-2011.

Ferrare, R., D. Turner, M. Clayton, B. Schmid, J. Redemann, D. Covert, R. Elleman, J. Ogren, E. Andrews, J. E. M. Goldsmith, and H. Jonsson (2006), Evaluation of daytime measurements of aerosols and water vapor made by an operational Raman lidar over the Southern Great Plains, *J. Geophys. Res.*, *111*(D5), doi:10.1029/2005JD005836.

Getzewich, B. J., J. L. Tackett, J. Kar, A. Garnier, M. A. Vaughan, and B. Hunt (2016), CALIOP Calibration: Version 4.0 Algorithm Updates, *EPJ Web of Conferences*, *119*, 04,013, doi:10.1051/epjconf/201611904013.

Goldsmith, J. E. M., F. H. Blair, S. E. Bisson, and D. D. Turner (1998), Turn-Key Raman Lidar for Profiling Atmospheric Water Vapor, Clouds, and Aerosols, *Appl. Opt.*, *37*(21), 4979–4990, doi:10.1364/AO.37.004979.

Hair, J. W., C. A. Hostetler, A. L. Cook, D. B. Harper, R. A. Ferrare, T. L. Mack, W. Welch, L. R. Izquierdo, and F. E. Hovis (2008), Airborne High Spectral Resolution Lidar for profiling aerosol optical properties, *Appl. Opt.*, *47*(36), 6734–6752, doi:10.1364/AO.47.006734.

Hu, Y. (2007), Depolarization ratio–effective lidar ratio relation: Theoretical basis for space lidar cloud phase discrimination, *Geophys. Res. Lett.*, *34*(11), doi:10.1029/2007gl029584.

Huang, J., Q. Fu, J. Su, Q. Tang, P. Minnis, Y. Hu, Y. Yi, and Q. Zhao (2009), Taklimakan dust aerosol radiative heating derived from CALIPSO observations using the Fu-Liou radiation model with CERES constraints, *Atmos. Chem. Phys.*, *9*(12), 4011–4021, doi:10.5194/acp-9-4011-2009.

Illingworth, A. J., H. W. Barker, A. Beljaars, M. Ceccaldi, H. Chepfer, N. Clerbaux, J. Cole, J. Delanoë, C. Domenech, D. P. Donovan, and et al. (2015), The EarthCARE Satellite: The Next Step Forward in Global Measurements of Clouds, Aerosols, Precipitation, and Radiation, *Bull. Amer. Meteor. Soc.*, *96*(8), 1311–1332, doi:10.1175/bams-d-12-00227.1.

Jethva, H., O. Torres, L. A. Remer, and P. K. Bhartia (2013), A Color Ratio Method for Simultaneous Retrieval of Aerosol and Cloud Optical Thickness of Above-Cloud Absorbing Aerosols From Passive Sensors: Application to MODIS Measurements, *IEEE Trans. Geosci. Remote Sens.*, *51*(7), 3862–3870, doi:10.1109/tgrs.2012.2230008.

Josset, D., J. Pelon, A. Protat, and C. Flamant (2008), New approach to determine aerosol optical depth from combined CALIPSO and CloudSat ocean surface echoes, *Geophys. Res. Lett.*, *35*(10), doi:10.1029/2008gl033442.

Kacenelenbogen, M., J. Redemann, M. A. Vaughan, A. H. Omar, P. B. Russell, S. Burton, R. R. Rogers, R. A. Ferrare, and C. A. Hostetler (2014), An evaluation of CALIOP/CALIPSO's aerosol-above-cloud detection and retrieval capability over North America, *J. Geophys. Res.*, *119*(1), 230–244, doi:10.1002/2013jd020178.

Kim, M.-H., A. H. Omar, M. A. Vaughan, D. M. Winker, C. R. Trepte, Y. Hu, Z. Liu, and S.-W. Kim (2017), Quantifying the low bias of CALIPSO's column aerosol opti-

cal depth due to undetected aerosol layers, *J. Geophys. Res.*, *122*(2), 1098–1113, doi:10.1002/2016jd025797.

Kokhanovsky, A. A., J. L. Deuzé, D. J. Diner, O. Dubovik, F. Ducos, C. Emde, M. J. Garay, R. G. Grainger, A. Heckel, M. Herman, and et al. (2010), The inter-comparison of major satellite aerosol retrieval algorithms using simulated intensity and polarization characteristics of reflected light, *Atmos. Meas. Tech.*, *3*(4), 909–932, doi:10.5194/amt-3-909-2010.

Lacagnina, C., O. P. Hasekamp, and O. Torres (2017), Direct radiative effect of aerosols based on PARASOL and OMI satellite observations, *J. Geophys. Res.*, *122*(4), 2366–2388, doi:10.1002/2016jd025706.

Li, Z., X. Zhao, R. Kahn, M. Mishchenko, L. Remer, K.-H. Lee, M. Wang, I. Laszlo, T. Nakajima, and H. Maring (2009), Uncertainties in satellite remote sensing of aerosols and impact on monitoring its long-term trend: a review and perspective, *Ann. Geophys.*, *27*(7), 2755–2770, doi:10.5194/angeo-27-2755-2009.

Liu, Z., M. Vaughan, D. Winker, C. Kittaka, B. Getzewich, R. Kuehn, A. Omar, K. Powell, C. Trepte, and C. Hostetler (2009), The CALIPSO Lidar Cloud and Aerosol Discrimination: Version 2 Algorithm and Initial Assessment of Performance, *J. Atmos. Oceanic Technol.*, *26*(7), 1198–1213, doi:10.1175/2009JTECHA1229.1.

Liu, Z., D. Winker, A. Omar, M. Vaughan, J. Kar, C. Trepte, Y. Hu, and G. Schuster (2015), Evaluation of CALIOP 532 nm aerosol optical depth over opaque water clouds, *Atmos. Chem. Phys.*, *15*(3), 1265–1288, doi:10.5194/acp-15-1265-2015.

Lyapustin, A., J. Martonchik, Y. Wang, I. Laszlo, and S. Korkin (2011a), Multiangle implementation of atmospheric correction (MAIAC): 1. Radiative transfer basis and look-up tables, *J. Geophys. Res.*, *116*(D3), doi:10.1029/2010jd014985.

Lyapustin, A., Y. Wang, I. Laszlo, R. Kahn, S. Korkin, L. Remer, R. Levy, and J. S. Reid (2011b), Multiangle implementation of atmospheric correction (MAIAC): 2. Aerosol algorithm, *J. Geophys. Res.*, *116*(D3), doi:10.1029/2010jd014986.

Matus, A. V., T. S. L'Ecuyer, J. E. Kay, C. Hannay, and J.-F. Lamarque (2015), The Role of Clouds in Modulating Global Aerosol Direct Radiative Effects in Spaceborne Active Observations and the Community Earth System Model, *J. Climate*, *28*(8), 2986–3003, doi:10.1175/jcli-d-14-00426.1.

McGill, M. J., J. E. Yorks, V. S. Scott, A. W. Kupchock, and P. A. Selmer (2015), The Cloud-Aerosol Transport System (CATS): a technology demonstration on the International Space Station, *Lidar Remote Sensing for Environmental Monitoring XV*, doi:10.1117/12.2190841.

Meyer, K., S. Platnick, and Z. Zhang (2015), Simultaneously inferring above-cloud absorbing aerosol optical thickness and underlying liquid phase cloud optical and microphysical properties using MODIS, *J. Geophys. Res.*, *120*(11), 5524–5547, doi:10.1002/2015jd023128.

Müller, D., C. A. Hostetler, R. A. Ferrare, S. P. Burton, E. Chemyakin, A. Kolgotin, J. W. Hair, A. L. Cook, D. B. Harper, R. R. Rogers, and et al. (2014), Airborne Multiwavelength High Spectral Resolution Lidar (HSRL-2) observations during TCAP 2012: vertical profiles of optical and microphysical properties of a smoke/urban haze plume over the northeastern coast of the US, *Atmospheric Measurement Techniques*, *7*(10), 3487–3496, doi:10.5194/amt-7-3487-2014.

Newsom, R. (2009), Raman Lidar (RL) Handbook, *Tech. Rep. DOE/SC-ARM/TR-038*, U.S. Department of Energy.

Oikawa, E., T. Nakajima, T. Inoue, and D. Winker (2013), A study of the shortwave direct aerosol forcing using ESSP/CALIPSO observation and GCM simulation, *J. Geophys. Res.*, *118*(9), 3687–3708, doi:10.1002/jgrd.50227.

Pappalardo, G., U. Wandinger, L. Mona, A. Hiebsch, I. Mattis, A. Amodeo, A. Ansmann, P. Seifert, H. Linné, A. Apituley, and et al. (2010), EARLINET correlative measurements for CALIPSO: First intercomparison results, *J. Geophys. Res.*, *115*, doi:10.1029/2009jd012147.

Rogers, R. R., M. A. Vaughan, C. A. Hostetler, S. P. Burton, R. A. Ferrare, S. A. Young, J. W. Hair, M. D. Obland, D. B. Harper, A. L. Cook, and et al. (2014), Looking through the haze: evaluating the CALIPSO level 2 aerosol optical depth using airborne high spectral resolution lidar data, *Atmos. Meas. Tech.*, *7*(12), 4317–4340, doi:10.5194/amt-7-4317-2014.

Thorsen, T. J., and Q. Fu (2015a), Automated Retrieval of Cloud and Aerosol Properties from the ARM Raman Lidar. Part II: Extinction, *J. Atmos. Oceanic Technol.*, *32*(11), 1999–2023, doi:10.1175/jtech-d-14-00178.1.

Thorsen, T. J., and Q. Fu (2015b), CALIPSO-inferred aerosol direct radiative effects: bias estimates using ground-based Raman lidars, *J. Geophys. Res. Atmos.*, *120*(12), 12,209–12,220, doi:10.1002/2015jd024095.

Thorsen, T. J., Q. Fu, R. K. Newsom, D. D. Turner, and J. M. Comstock (2015), Automated Retrieval of Cloud and Aerosol Properties from the ARM Raman Lidar. Part I: Feature Detection, *J. Atmos. Oceanic Technol.*, *32*(11), 1977–1998, doi:10.1175/jtech-d-14-00150.1.

Torres, O., A. Tanskanen, B. Veihelmann, C. Ahn, R. Braak, P. K. Bhartia, P. Veefkind, and P. Levelt (2007), Aerosols and surface UV products from Ozone Monitoring Instrument observations: An overview, *J. Geophys. Res.*, *112*(D24), doi:10.1029/2007jd008809.

Vaughan, M. A., D. M. Winker, and K. A. Powell (2005), CALIOP Algorithm Theoretical Basis Document Part 2: Feature Detection and Layer Properties Algorithms, *Tech. rep.*, NASA Langley Research Center.

Venkata, S., and J. Reagan (2016), Aerosol Retrievals from CALIPSO Lidar Ocean Surface Returns, *Remote Sensing*, *8*(12), 1006, doi:10.3390/rs8121006.

Waquet, F., J. Riedi, L. C. Labonnote, P. Goloub, B. Cairns, J.-L. Deuzé, and D. Tanré (2009), Aerosol Remote Sensing over Clouds Using A-Train Observations, *J. Atmos. Sci.*, *66*(8), 2468–2480, doi:10.1175/2009jas3026.1.

Waquet, F., C. Cornet, J.-L. Deuzé, O. Dubovik, F. Ducos, P. Goloub, M. Herman, T. Lapyonok, L. C. Labonnote, J. Riedi, and et al. (2013), Retrieval of aerosol microphysical and optical properties above liquid clouds from POLDER/PARASOL polarization measurements, *Atmos. Meas. Tech.*, *6*(4), 991–1016, doi:10.5194/amt-6-991-2013.

Winker, D. M., M. A. Vaughan, A. Omar, Y. Hu, K. A. Powell, Z. Liu, W. H. Hunt, and S. A. Young (2009), Overview of the CALIPSO mission and CALIOP data processing algorithms, *J. Atmos. Oceanic Technol.*, doi:10.1175/2009JTECHA1281.1.

Winker, D. M., P. J., J. Coakley Jr., S. Ackerman, R. Charlson, P. Colarco, P. Flamant, F. Q., R. Hoff, C. Kittaka, T. Kubar, H. LeTruet, M. McCormick, G. Megie, L. Poole, K. Powell, C. Trepte, M. Vaughan, and B. A. Wielicki (2010), The CALIPSO Mission: A Global 3d View Of Aerosols And Clouds, *Bull. Amer. Meteor. Soc.*, doi:10.1175/2009JTECHA1281.1.

Yorks, J. E., M. J. McGill, S. P. Palm, D. L. Hlavka, P. A. Selmer, E. P. Nowottnick, M. A. Vaughan, S. D. Rodier, and W. D. Hart (2016), An overview of the CATS level 1 processing algorithms and data products, *Geophys. Res. Lett.*, *43*(9), 4632–4639, doi:10.1002/2016gl068006.

Yu, H., Y. J. Kaufman, M. Chin, G. Feingold, L. A. Remer, T. L. Anderson, Y. Balkanski, N. Bellouin, O. Boucher, S. Christopher, and et al. (2006), A review of measurement-based assessments of the aerosol direct radiative effect and forcing, *Atmos. Chem. Phys.*, *6*(3), 613–666, doi:10.5194/acp-6-613-2006.

Zarzycki, C. M., and T. C. Bond (2010), How much can the vertical distribution of black carbon affect its global direct radiative forcing?, *Geophys. Res. Lett.*, *37*(20), doi:10.1029/2010gl044555.

Supporting Information for

"Towards quantifying global aerosol direct radiative effects using lidar: detection sensitivity"

Tyler J. Thorsen[1], Richard A. Ferrare[1], Chris A. Hostetler[1], Mark A. Vaughan[1], and Qiang Fu[2]

[1]NASA Langley Research Center, Mail Stop 420, Hampton, Virginia, USA

[2]Department of Atmospheric Sciences, University of Washington, Seattle, Washington, USA

Contents

Text S1–S5, Figures S1–S3 and captions, Table S1 and caption.

S1 Dataset descriptions and collocation

The ARM Raman lidar (RL) measures elastic backscattered light at 355 nm, Raman backscattered light from nitrogen and water vapor molecules, and has rotational Raman temperature channels [*Goldsmith et al.*, 1998; *Ferrare et al.*, 2006; *Newsom*, 2009]. We use the Feature detection and EXtinction retrieval (FEX) algorithm [*Thorsen et al.*, 2015; *Thorsen and Fu*, 2015a] data (RL-FEX) that provides retrievals of cloud and aerosols from this system at a 2 min time resolution and 30 m vertical resolution. RL-FEX data from December 2010 – December 2014 at the ARM Tropical Western Pacific (TWP) Darwin, Australia site (12.43° S, 130.89° E) and from August 2008 – August 2013 at the Southern Great Plains (SGP) site in Oklahoma (36.61° N, 97.49° W) are used in this study.

The CALIPSO satellite [*Winker et al.*, 2009, 2010] provides near-global observations in a sun-synchronous orbit at approximately 0130 and 1330 (local time). The main instrument on board is CALIOP, a 2 wavelength (532 nm and 1064 nm) polarization-sensitive lidar [*Hunt et al.*, 2009]. We use the CALIPSO level 2 version 3 (v3) and version 4 (v4) vertical feature mask (VFM) and aerosol layer (ALay) product.

The RL-FEX and CALIPSO data are collocated by taking the set of CALIPSO profiles that fall within 200 km of the ARM sites and the RL profiles that fall within ±2 hours of

Corresponding author: Tyler J. Thorsen, tyler.thorsen@nasa.gov

CALIPSO overpass times. Since aerosol properties are typically homogeneous at scales of less than 10 h and 200 km [*Anderson et al.*, 2003] we expect the lack of direct collocation to minimally affect our comparisons. This is confirmed by examining CALIPSO (RL-FEX) AOD and aerosol occurrence profiles. Both show no significant dependence on distance (time) within the spatial (temporal) collocation criteria (not shown).

Our analysis is focused on the subset of profiles that are transparent, i.e. profiles where the laser beam penetrates completely through all cloud and aerosol layers. Only in transparent profiles can we expect all aerosol in the column to be detected. For CALIPSO data products, transparent profiles are defined as those with the presence of a signal return from the surface. In the RL-FEX product, transparent profiles are defined as those where the elastic channel signal-to-noise ratio (SNR) is greater than 1 at 18.5 km. Addition comparisons are also made in cloud-free profiles, i.e. profiles that are both transparent and have no cloud layers detected.

Data from the airborne NASA Langley HSRL [*Hair et al.*, 2008] over 25 field campaigns across North America (Fig. S1 and Table S1) are also used in the this study. The airborne NASA HSRL uses the HSRL technique [*Grund and Eloranta*, 1991] to measure extinction and backscatter coefficients independently at 532nm along with the standard backscatter technique at 1064nm. Profiles of aerosol extinction and backscatter are averaged to 1 min (~6 km along track of the aircraft) and 30 m vertically. A second iteration of this instrument, HSRL-2, added HSRL capacity at 355nm and began flying in field missions in 2012.

S2 Degrading the RL-FEX data to a CALIPSO-like detection sensitivity

A direct comparison of the RL-FEX AOD and CALIPSO AOD is complicated by a difference in wavelength between the two instruments (355nm compared to 532nm) and the additional uncertainty from CALIPSO's selection of the lidar ratio. Therefore, the methodology of *Thorsen and Fu* [2015b] is used to compute the AOD difference due solely to the difference in detection sensitivity between the two instruments. The *Thorsen and Fu* [2015b] method produces a RL-FEX dataset that is degraded to the sensitivity of CALIPSO. In brief, the difference in the aerosol occurrence profiles in each collocated overpass are used to compute the probability that CALIPSO does not detect aerosol. These per-pass probability profiles are then applied to the RL-FEX data using a Monte Carlo method to produce many (1000) realizations of CALIPSO-like aerosol profiles. Biases from aerosol undetected by

CALIPSO can then be assessed by comparing the original RL-FEX data to simulated CALIPSO-like data and statistical significance is assess from the individual Monte Carlo samples. The methodology of *Thorsen and Fu* [2015b] is also extended to compute the portion of the AOD bias due to all aerosol in the profile going completely undetected by CALIPSO (i.e. AOD = 0). The probability that all aerosol goes completely undetected is computed for each collected overpass by noting the fraction of CALIPSO profiles with zero AOD. This probably is then applied to the RL-FEX data in the overpass to generate 1000 Monte Carlo sets of RL-FEX data with the same fraction of profiles with no AOD.

S3 Detection sensitivity of ARM RL and NASA HSRL datasets

The usefulness of the threshold analysis in section 5 is predicated on the ability of the ARM RL and NASA HSRL to detect all aerosol that contribute significantly to the AOD. Comparisons of data from both these instruments to the Aerosol Robotic Network project (AERONET) [*Holben et al.*, 1998] suggest that this is the case with AOD typically differing by less than a few percent [*Thorsen and Fu*, 2015a; *Rogers et al.*, 2009]. Figure S2 also supports that these datasets capture all the radiatively significant aerosol. The aerosol backscatter cumulative distribution functions (CDF, blue lines) are shifted towards smaller backscatter values relative to the AOD biases. This shows that there is a portion of aerosols detected in these lidar datasets that only contribute minimally to the total AOD (and hence are radiatively-insignificant). For example, 10% of the weakest-scattering aerosols only contribute about 1% of the total AOD in all three datasets.

S4 Backscatter color ratio

The AOD bias as a function of the aerosol backscatter detection threshold are derived from both the ARM RL measurements at 355nm and the NASA airborne HSRL measurements at 532nm (section 5). To facilitate comparisons between the two, the aerosol backscatter color ratio, i.e. the ratio of the backscatter coefficient at 355nm to 532nm, is computed from data taken during the Combined HSRL And Raman lidar Measurement Study (CHARMS). CHARMS occurred from July through September 2015 at the ARM SGP site during which the University of Wisconsin bagoHSRL operated along side the ARM RL. The UW bagoHSRL measures aerosol backscatter profiles at both 532 and 1064 nm, and aerosol extinction profiles at 532 nm using the HSRL technique [*Grund and Eloranta*, 1991]. From combination of ARM RL and UW bagoHSRL data the mean 355nm/532nm aerosol

backscatter color ratio is found to be 1.60 (with a standard deviation of 0.60). This ratio of 1.60 is used to convert 355nm (532nm) values derived from the ARM RL (NASA HSRL) data to 532nm (355nm) and to offset the bottom and top x axes in Figs. 4, S2.

S5 Comparisons to other estimates of CALIPSO's detection sensitivity

Kim et al. [2017] estimated CALIPSO's AOD bias due to undetected aerosol in cloud-free profiles globally using "full-column" retrievals. Instead of obtaining AOD by integrating only the aerosol layers identified by CALIPSO's detection algorithm, a full-column retrieval integrates the entire backscatter profile. Using this technique, *Kim et al.* [2017] show that CALIPSO underestimates the global mean AOD in cloud-free profiles by 21% at night and 32% during the day. The *Kim et al.* [2017] nighttime bias estimate is very similar that made in this study (-22%) while their daytime values is smaller than our estimate of -47%. This daytime discrepancy could be due to an under sampling on our part of the solar background conditions that CALIPSO experiences globally, or possibly due to uncertainties in the full-column retrievals. As *Kim et al.* [2017] show, full-column retrievals are very sensitive to both calibration, and, since CALIPSO measures attenuated backscatter, the accuracy of the lidar ratio used for the undetected aerosol.

Rogers et al. [2014] determined median CALIPSO detection threshold in cloud-free situations through collocated comparisons to NASA airborne HSRL datasets. Good agreement exists between this study and the *Rogers et al.* [2014] estimate of CALIPSO's daytime detection thresholds: *Rogers et al.* [2014] derive a daytime threshold of $1.7x10^{-3}km^{-1}sr^{-1}$ compared to our estimate of $1.5x10^{-3}km^{-1}sr^{-1}$ (at 532nm). However, the nighttime threshold inferred by this study ($7.7x10^{-4}km^{-1}sr^{-1}$ at 532nm) is larger than *Rogers et al.* [2014] ($3.1x10^{-4}km^{-1}sr^{-1}$ at 532nm). This discrepancy at nighttime may be partially due to the sampling by *Rogers et al.* [2014] who analyzed more than two times less nighttime data than daytime. This is also the opposite agreement found between our study and *Kim et al.* [2017] whose estimate of CALIPSO AOD bias at night agrees well while our daytime estimate is larger.

Figures S1–S3

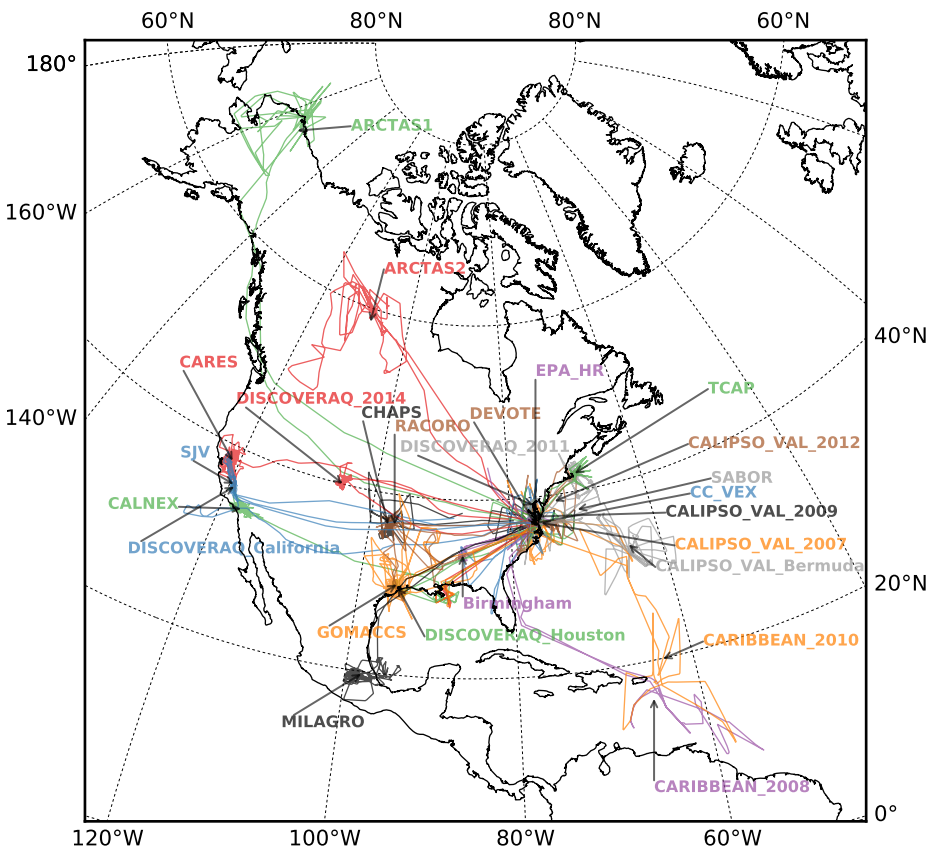

Figure S1. Ground-tracks of the NASA Langley airborne HSRL campaigns used in this study.

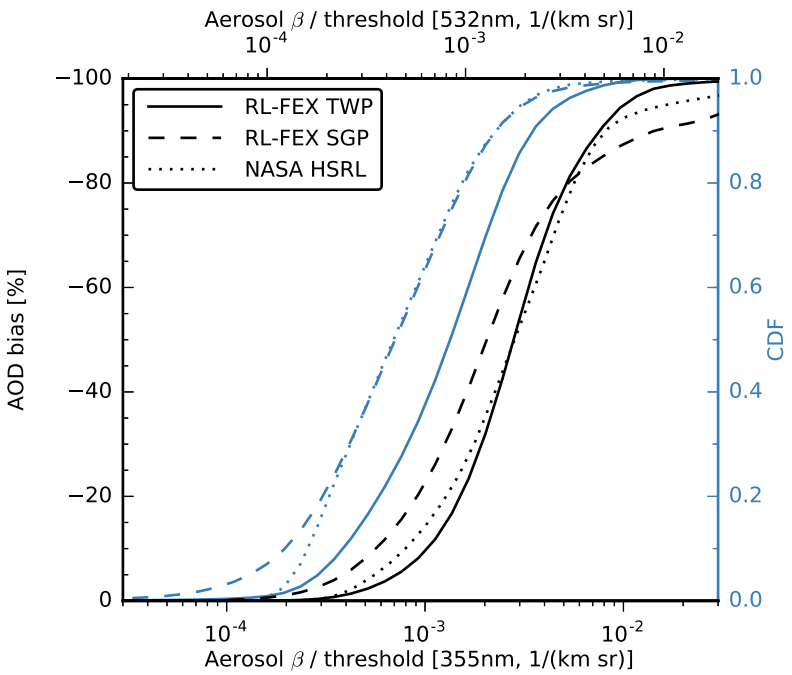

Figure S2. The aerosol optical depth (AOD) bias as a function of imposing a minimum detectable aerosol backscatter (β) threshold on the RL-FEX TWP (solid black), RL-FEX SGP (dashed black), and NASA Langley HSRL (dotted black) datasets. The NASA Langley HSRL is the compilation of 25 field campaigns (Fig. S1). Also shown is the cumulative distribution functions (blue) of the aerosol backscatter from each dataset. The bottom (top) x axis in give the backscatter at 355nm (532nm). These 355nm/532nm axes are offset using a backscatter color ratio of 1.60 (Text S4).

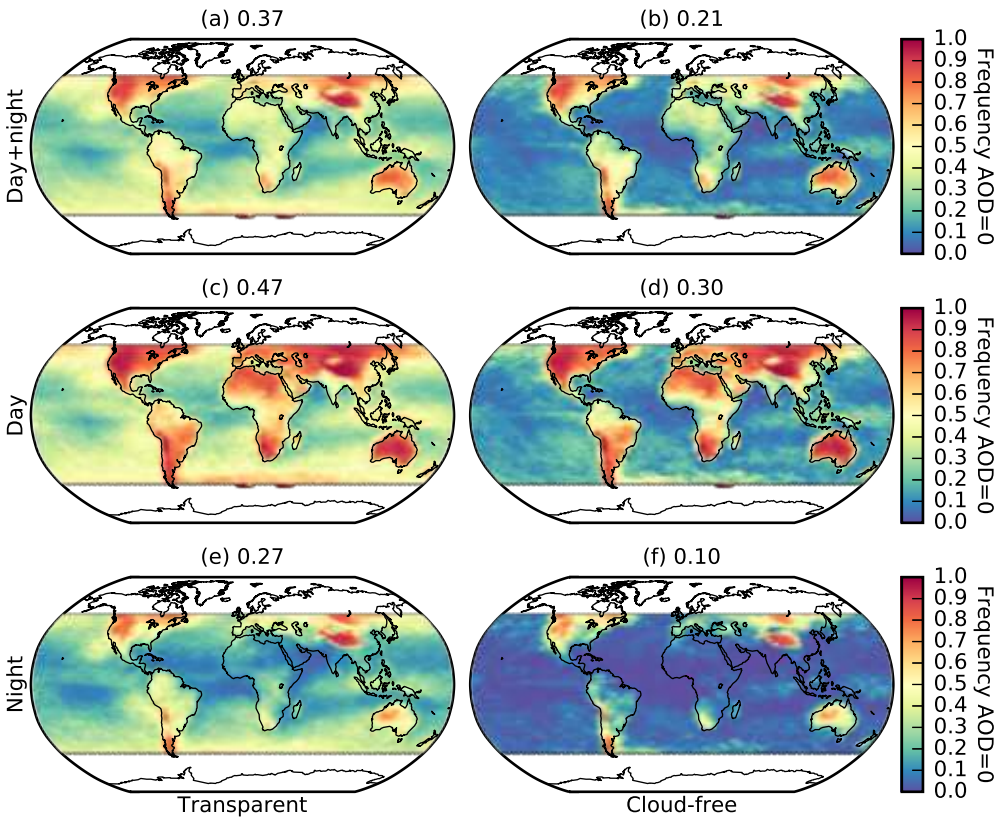

Figure S3. The frequency of no aerosol optical depth (i.e. AOD = 0) in the CATS 5km Lay M7.2 v1.05 product for (a,c,e) transparent and (b,d,f) cloud-free profiles during (a,b) both day and night, (c,d) day only, and (e,f) night only. The global mean frequency of AOD = 0 is given above each panel. Average frequencies are shown on a 2° by 5° latitude by longitude grid from the period of March 2015 - February 2017.

Table S1

Table S1. List of NASA Langley airborne HSRL campaigns used in this study.

Field Mission	Dates	Location
MILAGRO	March 2006	Mexico City
CALIPSO Validation (CC_VEX)	May – August 2006	Southeastern US
GOMACCS	September 2006	Houston
San Joaquin Valley (SJV)	February 2007	California
CHAPS	June 2007	Oklahoma
CALIPSO Validation (CALIPSO_VAL_2007)	January 2007, August 2007	Eastern US
Caribbean 2008	January – February 2008	Caribbean
ARCTAS 1	April 2008	Alaska
ARCTAS 2	June – July 2008	Northwest Canada
Birmingham	September – October 2008	Alabama
CALIPSO Validation (CALIPSO_VAL_2009)	January 2009, April 2009	Eastern US
RACORO	June 2009	Oklahoma
CalNEX	May 2010	Los Angeles
CARES	June 2010	Sacramento
Caribbean 2010	August 2010	Caribbean
DISCOVER-AQ 2011	July 2011	DC-Baltimore
EPA_HR	August 2011	Southeastern Virginia
DEVOTE	October 2011	Southeastern US
CALIPSO Validation (CALIPSO_VAL_2012)	March 2012	Eastern US
TCAP[a]	July 2012	Cape Cod
DISCOVER-AQ California[a]	January – February 2013	Central California
DISCOVER-AQ Houston[a]	September 2013	Houston
CALIPSO Validation (CALIPSO_VAL_Bermuda)	June 2014	Eastern US, Bermuda
SABOR	July – August 2014	Atlantic Ocean
DISCOVER-AQ 2014[a]	July – August 2014	Denver

[a]HSRL-2 instrument

References

Anderson, T. L., R. J. Charlson, D. M. Winker, J. A. Ogren, and K. Holmén (2003), Mesoscale Variations of Tropospheric Aerosols, *J. Atmos. Sci.*, *60*(1), 119–136, doi:10.1175/1520-0469(2003)060<0119:mvota>2.0.co;2.

Ferrare, R., D. Turner, M. Clayton, B. Schmid, J. Redemann, D. Covert, R. Elleman, J. Ogren, E. Andrews, J. E. M. Goldsmith, and H. Jonsson (2006), Evaluation of daytime measurements of aerosols and water vapor made by an operational Raman lidar over the Southern Great Plains, *J. Geophys. Res.*, *111*(D5), doi:10.1029/2005JD005836.

Goldsmith, J. E. M., F. H. Blair, S. E. Bisson, and D. D. Turner (1998), Turn-Key Raman Lidar for Profiling Atmospheric Water Vapor, Clouds, and Aerosols, *Appl. Opt.*, *37*(21), 4979–4990, doi:10.1364/AO.37.004979.

Grund, C. J., and E. W. Eloranta (1991), University of Wisconsin High Spectral Resolution Lidar, *Opt. Eng.*, *30*, 6–12.

Hair, J. W., C. A. Hostetler, A. L. Cook, D. B. Harper, R. A. Ferrare, T. L. Mack, W. Welch, L. R. Izquierdo, and F. E. Hovis (2008), Airborne High Spectral Resolution Lidar for profiling aerosol optical properties, *Appl. Opt.*, *47*(36), 6734–6752, doi:10.1364/AO.47.006734.

Holben, B., T. Eck, I. Slutsker, D. Tanre, J. Buis, A. Setzer, E. Vermote, J. Reagan, Y. Kaufman, T. Nakajima, F. Lavenu, I. Jankowiak, and A. Smirnov (1998), AERONET— A Federated Instrument Network and Data Archive for Aerosol Characterization, *Remote Sens. Environ.*, *66*(1), 1 – 16, doi:10.1016/S0034-4257(98)00031-5.

Hunt, W. H., D. M. Winker, M. A. Vaughan, K. A. Powell, P. L. Lucker, and C. Weimer (2009), CALIPSO Lidar Description and Performance Assessment, *J. Atmos. Oceanic Technol.*, *26*(7), 1214–1228, doi:10.1175/2009JTECHA1223.1.

Kim, M.-H., A. H. Omar, M. A. Vaughan, D. M. Winker, C. R. Trepte, Y. Hu, Z. Liu, and S.-W. Kim (2017), Quantifying the low bias of CALIPSO's column aerosol optical depth due to undetected aerosol layers, *J. Geophys. Res.*, *122*(2), 1098–1113, doi:10.1002/2016jd025797.

Newsom, R. (2009), Raman Lidar (RL) Handbook, *Tech. Rep. DOE/SC-ARM/TR-038*, U.S. Department of Energy.

Rogers, R. R., J. W. Hair, C. A. Hostetler, R. A. Ferrare, M. D. Obland, A. L. Cook, D. B. Harper, S. P. Burton, Y. Shinozuka, C. S. McNaughton, and et al. (2009), NASA LaRC airborne high spectral resolution lidar aerosol measurements during MILAGRO: obser-

vations and validation, *Atmos. Chem. Phys.*, *9*(14), 4811–4826, doi:10.5194/acp-9-4811-2009.

Rogers, R. R., M. A. Vaughan, C. A. Hostetler, S. P. Burton, R. A. Ferrare, S. A. Young, J. W. Hair, M. D. Obland, D. B. Harper, A. L. Cook, and et al. (2014), Looking through the haze: evaluating the CALIPSO level 2 aerosol optical depth using airborne high spectral resolution lidar data, *Atmos. Meas. Tech.*, *7*(12), 4317–4340, doi:10.5194/amt-7-4317-2014.

Thorsen, T. J., and Q. Fu (2015a), Automated Retrieval of Cloud and Aerosol Properties from the ARM Raman Lidar. Part II: Extinction, *J. Atmos. Oceanic Technol.*, *32*(11), 1999–2023, doi:10.1175/jtech-d-14-00178.1.

Thorsen, T. J., and Q. Fu (2015b), CALIPSO-inferred aerosol direct radiative effects: bias estimates using ground-based Raman lidars, *J. Geophys. Res. Atmos.*, *120*(12), 12,209–12,220, doi:10.1002/2015jd024095.

Thorsen, T. J., Q. Fu, R. K. Newsom, D. D. Turner, and J. M. Comstock (2015), Automated Retrieval of Cloud and Aerosol Properties from the ARM Raman Lidar. Part I: Feature Detection, *J. Atmos. Oceanic Technol.*, *32*(11), 1977–1998, doi:10.1175/jtech-d-14-00150.1.

Winker, D. M., M. A. Vaughan, A. Omar, Y. Hu, K. A. Powell, Z. Liu, W. H. Hunt, and S. A. Young (2009), Overview of the CALIPSO mission and CALIOP data processing algorithms, *J. Atmos. Oceanic Technol.*, doi:10.1175/2009JTECHA1281.1.

Winker, D. M., P. J., J. Coakley Jr., S. Ackerman, R. Charlson, P. Colarco, P. Flamant, F. Q., R. Hoff, C. Kittaka, T. Kubar, H. LeTruet, M. McCormick, G. Megie, L. Poole, K. Powell, C. Trepte, M. Vaughan, and B. A. Wielicki (2010), The CALIPSO Mission: A Global 3d View Of Aerosols And Clouds, *Bull. Amer. Meteor. Soc.*, doi:10.1175/2009JTECHA1281.1.